Methods xxx (2014) xxx–xxx

Contents lists available at ScienceDirect

Methods

journal homepage: www.elsevier.com/locate/ymeth

Spatial mapping of structural and connectional imaging data for the developing human brain with diffusion tensor imaging

Austin Ouyang [a], Tina Jeon [a], Susan M. Sunkin [b], Mihovil Pletikos [c], Goran Sedmak [c,d], Nenad Sestan [c], Ed S. Lein [b], Hao Huang [a,e,*]

[a] Advanced Imaging Research Center, University of Texas Southwestern Medical Center, Dallas, TX 75390, United States
[b] Allen Institute for Brain Science, Seattle, WA, United States
[c] Department of Neurobiology and Kavli Institute for Neuroscience, Yale University School of Medicine, New Haven, CT 06510, United States
[d] University of Zagreb School of Medicine, Croatian Institute for Brain Research, Salata 12, 10 000 Zagreb, Croatia
[e] Department of Radiology, University of Texas Southwestern Medical Center, Dallas, TX 75390, United States

ARTICLE INFO

Article history:
Received 15 March 2014
Received in revised form 8 September 2014
Accepted 21 October 2014
Available online xxxx

Keywords:
Human brain development
Fetal brain
DTI
Tractography
Connection
Cortical mapping

ABSTRACT

During human brain development from fetal stage to adulthood, the white matter (WM) tracts undergo dramatic changes. Diffusion tensor imaging (DTI), a widely used magnetic resonance imaging (MRI) modality, offers insight into the dynamic changes of WM fibers as these fibers can be noninvasively traced and three-dimensionally (3D) reconstructed with DTI tractography. The DTI and conventional T1 weighted MRI images also provide sufficient cortical anatomical details for mapping the cortical regions of interests (ROIs). In this paper, we described basic concepts and methods of DTI techniques that can be used to trace major WM tracts noninvasively from fetal brain of 14 postconceptional weeks (pcw) to adult brain. We applied these techniques to acquire DTI data and trace, reconstruct and visualize major WM tracts during development. After categorizing major WM fiber bundles into five unique functional tract groups, namely limbic, brain stem, projection, commissural and association tracts, we revealed formation and maturation of these 3D reconstructed WM tracts of the developing human brain. The structural and connectional imaging data offered by DTI provides the anatomical backbone of transcriptional atlas of the developing human brain.

1. Introduction

Human brain development is a complex and fascinating biological process. Starting as a simple tubular structure, the human brain undergoes a series of cellular and molecular processes underlying both microstructural and macrostructural changes during development. These cellular and molecular processes are precisely modulated by differential gene expressions [e.g. 1–4]. Understanding dynamics of neuroanatomy is complementary to establishing transcriptional atlas of the developing brain. Histology has been a dominant modality and remains to be an important method to study the detailed neural structures of developing brains [5–10]. Diffusion tensor imaging (DTI) [11], based on diffusion magnetic resonance imaging, has been effective to delineate the macrostructure and microstructure of developing brains. Compared to histology, DTI is noninvasive, three-dimensional (3D) and requires much less time to characterize the entire brain anatomy with the modern scanners. DTI based tractography can be used to effectively trace the major white matter (WM) tracts noninvasively. Structural and connectional data from DTI, therefore, can serve as the anatomical backbone for the transcriptional atlas of the developing brain.

Dramatic morphological changes of human brain take place during its development from early fetal stage to adulthood. The brain WM can be categorized into five tract groups based on their functions, namely, limbic, brain stem, projection, commissural and association tracts. In the prenatal early fetal stage such as 14 postconceptional weeks (pcw), most of traced major tracts with DTI tractography are brain stem and limbic tracts [12–15]. The 3D morphology of these traced WM tracts provides complementary information to the knowledge of WM obtained from histology at this age [e.g. 16,17]. More WM tracts in different tract groups can be appreciated with DTI tractography during fetal development until birth [12,13,18–20]. At birth, except the superior longitudinal fasciculus in the association tract group [e.g. 21], most other major WM tracts including short association tracts are well

* Corresponding author at: Advanced Imaging Research Center, University of Texas Southwestern Medical Center, 5323 Harry Hines Blvd., Dallas, TX 75390-8542, United States. Fax: +1 214 645 2744.
E-mail address: hao.huang@utsouthwestern.edu (H. Huang).

http://dx.doi.org/10.1016/j.ymeth.2014.10.025
1046-2023/

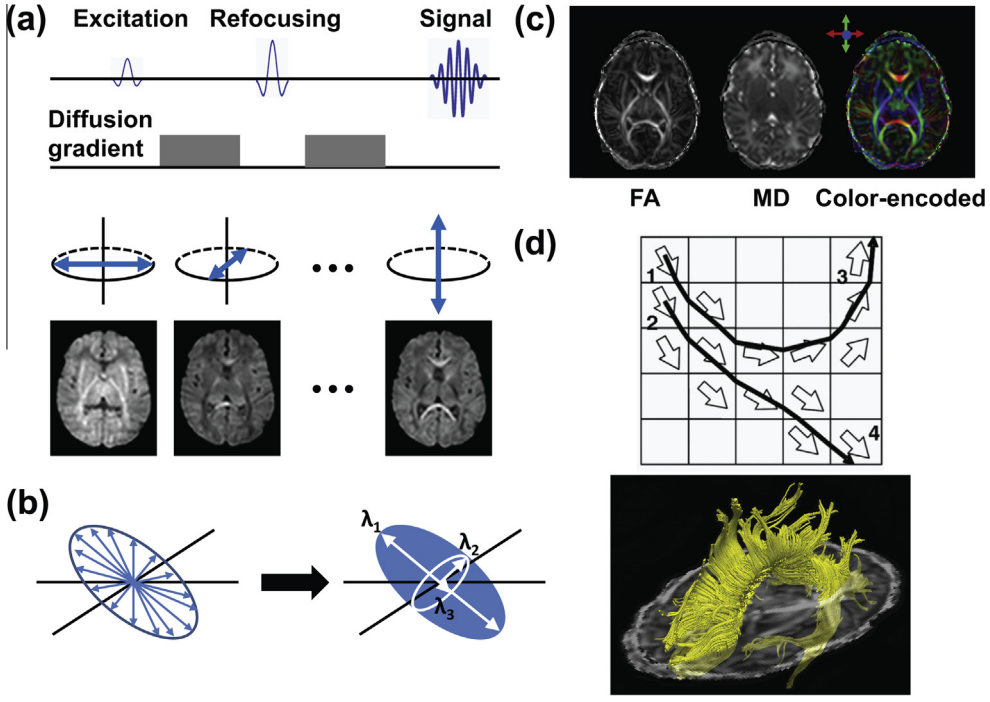

Fig. 1. (a) Typical Stejskal–Tanner diffusion sequence with the DWIs of a 37 pcw subject along the left–right, anterior–posterior, and inferior–superior directions. (b) Tensor fitting with the diffusion weighted image and diagonalization into the three eigenvalues and eigenvectors. (c) DTI-derived contrast maps with fractional anisotropy (FA), mean diffusivity, and color-encoded map from left to right. The red, green and blue color encodes orientation along left–right, anterior–posterior and inferior–superior, respectively. (d) DTI tractography with top panel showing the FACT algorithm and bottom panel presenting the traced corpus callosum using FACT.

developed [18,22] although many of them are not well myelinated. Postnatal WM development is associated with myelination, continuous maturation of part of the association fibers and elimination of another part of the short and unmyelinated fibers [23–28].

In this paper, we used DTI techniques to acquire data and trace, reconstruct and visualize major WM fibers of human brain during development from 14 pcw in the early fetal stage to adulthood. Qualitative morphological instead of quantitative microstructural changes (e.g. myelination or integrity enhancement characterized by measurement of DTI-derived metrics) of WM fibers were the focus of this study. After categorizing major WM fiber bundles into five tract groups, namely association, brain stem, projection, limbic and commissural tracts, we revealed formation and maturation of these 3D reconstructed WM tracts of the developing human brain by directly demonstrating the 3D morphological dynamics of these tracts. Below, we first described DTI techniques including concepts, acquisition method, tensor fitting and tractography protocols. We then showed 3D-reconstructed major WM tracts in each of the five categories for the developing brains from prenatal fetal stage to adulthood. The method of delineating 11 cortical regions of interests (ROIs) used for gene profiling and segmented from the cortical surface reconstructed with MRI data was also described. The advantages and limitations of the presented methods, specifically those related to DTI tractography, were discussed in the end.

2. Material and methods

2.1. DTI concepts and principles

DTI [11] is based on diffusion magnetic resonance imaging (MRI). MRI measures signals from ^{1}H (proton) nuclei which are magnetic spins in the magnetic field. In DTI studies, we can assume the signals are dominated by water protons. Diffusion magnetic resonance imaging measures water diffusion noninvasively by using the phase difference to detect water motion. Modern MR scanners are usually equipped with three orthogonal gradient systems in the X, Y and Z direction. They can also be used to measure diffusion. This function of the gradient systems is emphasized in Fig. 1a. A typical diffusion sequence [29] is featured with a pair of diffusion gradients placed on either side of the refocusing pulse, shown as Fig. 1a. The frequency of the water proton spin (ω) and the magnetic field B_0 have a simple relationship: $\omega = \gamma B_0$. By adding the gradient, the equation is changed to $\omega = \gamma(B_0 + \boldsymbol{G}(\boldsymbol{x})\cdot\boldsymbol{x})$ where $\boldsymbol{G}(\boldsymbol{x})$ is the gradient strength and $\boldsymbol{x}$ is the spatial location. After the first gradient, spins at different locations $\boldsymbol{x}$ have different frequencies and go out of phase as they "see" the different magnetic field strength ($B_0 + \boldsymbol{G}(\boldsymbol{x})\cdot\boldsymbol{x}$). With the second gradient, only the spin that does not move between two gradient lobes has perfect refocusing. Refocusing results in a strong signal which is bright in the acquired diffusion weighted images (DWI) (Fig. 1a). By combining the X, Y and Z gradients, we can apply the gradient along arbitrary directions. The blue arrows in Fig. 1a indicate the gradient directions. In human brain WM, water protons tend to move along the axons rather than perpendicular to them. When the diffusion gradient direction aligns with a specific axonal direction, the signal loss is displayed as dark intensities in the images. For example, the first gradient is applied along the horizontal direction (X direction) which is parallel to the axonal directions of the corpus callosum around midline of this axial brain image. Thus the corpus callosum area around the midline is dark in the correspondent diffusion weighted image. The amount of signal loss for those spins with movement is dependent on several parameters, the gradient strength G, the interval of the two gradients Δ and gradient duration δ. This can be described with the following equation:

$$\ln(S/S_0) = -\gamma^2 G^2 \delta^2 (\Delta - \delta/3) D \quad (1)$$

where D is diffusion coefficient, S and S_0 are the diffusion sensitized signal and non-diffusion signal. The complicated term $\gamma^2 G^2 \delta^2 (\Delta - \delta/3)$ can be simplified as a scalar b. Thus Eq. (1) can be simplified as $\ln(S/S_0) = -bD$.

As diffusion gradients can be applied to arbitrary directions, the diffusion profile composed of diffusion coefficients along these directions can be calculated. For simplification, the diffusion tensor is widely used to characterize the diffusion profile. Fig. 1b shows the tensor fitting process. Since a diffusion tensor has six degrees of freedom, at least six diffusion sensitized images need to be acquired to fit the tensor besides a non-diffusion image. The properties of the three-dimensional ellipsoid are usually defined by the following parameters, the length of the longest, middle and shortest axes (called eigenvalues λ_1, λ_2 and λ_3) and their orientations (called eigenvectors $\boldsymbol{v_1}$, $\boldsymbol{v_2}$ and $\boldsymbol{v_3}$), shown in Fig. 1b. As the three axes are orthogonal to each other, only six parameters, i.e. λ_1, λ_2, λ_3 and x, y, z component of $\boldsymbol{v_1}$, are independent.

Fractional anisotropy (FA) [30] has been widely used to characterize the anisotropy of the tensor. The equations of FA is as follows:

$$\mathrm{FA} = \frac{\sqrt{(\lambda_1-\lambda_2)^2+(\lambda_1-\lambda_3)^2+(\lambda_2-\lambda_3)^2}}{\sqrt{2}\sqrt{\lambda_1^2+\lambda_2^2+\lambda_3^2}} \quad (2)$$

DTI-derived FA map, mean diffusivity (MD) map, color-encoded map are shown in Fig. 1c. The values of FA range from 0 to 1. The FA map characterizes the shapes of the diffusion tensor. The higher the value of FA is, the more elongated the shape of diffusion ellipsoid looks like. The eigenvector associated with the largest eigenvalue ($\boldsymbol{v_1}$) can be used as an indicator of fiber orientation. DTI color-encoded map combines the information of FA and $\boldsymbol{v_1}$. In the colormap, red (R), green (G), and blue (B) colors are assigned to left–right, anterior–posterior, and superior–inferior orientations, respectively. The MD map depicts the size of diffusion ellipsoid. MD is a physical value and usually has the unit of 10^{-3} mm^2/s. Detailed review of DTI and its derived metrics can be found in the literature [31–33].

3D axonal bundles can be reconstructed from DTI data. The direction of the primary eigenvector ($\boldsymbol{v_1}$) of the tensor is believed to align with the orientation of its underlying organized structures. DTI-based tractography refers to the techniques of reconstructing the pathways of the WM tracts based on diffusion tensor information. Streamline propagation methods [34–40] are mostly used. DTI-based tractography requires a fractional anisotropy value higher than threshold and orientation continuity of the primary eigenvector. Upper panel of Fig. 1d shows the diagram of a widely used streamline tractography, fiber assignment by continuous tracking (FACT) [34], which connects the primary eigenvectors of diffusion tensors to reconstruct axonal pathways. Fiber tracings were initiated from voxel #1 and #2, respectively. With the restricting second region of interest (ROI) which is voxel #3 or #4, two lines were traced. An example of the 3D reconstructed 37 pcw-brain corpus callosum (yellow fibers) traced with this FACT algorithm is shown in the lower panel of Fig. 1d. Due to the fact that the diffusion tensor model oversimplifies complex neural structures inside the brain, many other tractography algorithms which adapt more sophisticated diffusion models rather than the tensor have been postulated. For major WM tracts, comparison of these DTI-based tractography and postmortem histological slides has shown that tractography based on DTI could reveal general morphology of major WM tracts reliably [41,42].

2.2. Prenatal brain specimens and postnatal healthy subjects

Three post mortem prenatal specimens were obtained from the University of Maryland Brain and Tissue Bank for Developmental Disorders (NICHD contract No. N01-HD-4-3368 and N01-HD-4-3383). Samples were fixed with 4% paraformaldehyde (PFA) in phosphate-buffered saline (PBS) and later used for acquisition of high resolution DTI data. In addition, one neonate, three children and one adult with no history of psychiatric or neurological disorders were recruited. The age, gender and race information of the prenatal brain specimens and postnatal healthy subjects that were utilized for annotation are shown in Table 1.

2.3. DTI data acquisition of postmortem samples

Postmortem prenatal brain specimens were kept immersed in fixation solution until 48 h before the MR experiments. Specimens were then transferred to PBS to wash out the fixative. Samples were then immersed in PBS in a custom-made MR compatible chamber throughout MR scanning. Three-dimensional multiple spin echo diffusion tensor imaging was performed in either an 11.7 T or 4.7 T Bruker scanner, depending on the size of the samples. The three-dimensional multiple echo (number of echoes = 8) sequence was adopted to improve the signal-to-noise ratio (SNR). The details of this three-dimensional multiple spin echo DTI sequence are displayed in Fig. 2. The 14 pcw prenatal brain was scanned in an 11.7 T Bruker scanner with a micro 2.5 30 mm inner diameter Bruker volume coil. The 17 pcw and 19 pcw prenatal brains were scanned in a 4.7 T Bruker scanner with a 70 mm inner diameter Bruker volume coil. These volume coils were used as both the radio frequency signal transmitter and receiver. A set of diffusion weighted images (DWI) were acquired in seven linearly independent directions. Diffusion sensitizing gradients with a b value of 1000 s/mm^2 were applied along six different orientations: [0.707,0.707,0], [0.707,0,0.707], [0,0.707,0.707], [−0.707, 0.707, 0], [0.707,0, −0.707], [0,−0.707,0.707]. DWI parameters for the 11.7 T scanner were: effective TE = 67 ms, TR = 0.8 s, FOV = 35 mm/28 mm/28 mm, imaging matrix = 128 × 80 × 80 (zero filled to data matrix = 128 × 128 × 128). The imaging resolution was 273 × 350 × 350 μm for the 14 pcw prenatal brain. DWI parameters for the 4.7 T scanner were: effective TE = 66 ms, TR = 0.8 s, FOV = 44–52 mm/40–46 mm/40–46 mm, imaging matrix = 128 × 72 × 72 (zero filled to data matrix = 128 × 128 × 128). The imaging resolution was 300–600 μm for the 17 pcw and 19 pcw prenatal brains. The total imaging time for each specimen was approximately 20 h per brain with two signal averages for DTI data acquisition at both 4.7 T and 11.7 T.

2.4. DTI data acquisition of in vivo healthy subjects

Two 3 T Philips Achieva MR systems, one located at Children's Medical Center (CMC) at Dallas and the other located at Advanced Imaging Research Center (AIRC) of University of Texas Southwestern Medical Center, were used to acquire DTI and T1 weighted image of the healthy subjects after birth. These two MR systems were equipped with the same gradients, console and 16-channel head coil for data acquisition of the subjects included in this study. The data

Table 1
Prenatal brain samples and postnatal healthy subjects.

Age	14 pcw	17 pcw	19 pcw	37 pcw	3 yrs	8 yrs	15 yrs	32 yrs
Gender	F	M	n/a	F	M	M	F	M
Race	Caucasian	Caucasian	Caucasian	Hispanic	Asian	Caucasian	Asian	Asian

Shaded time points indicate samples are from postmortem specimens. *Abbreviations*: pcw, post-conception weeks; years, postnatal years; F, female; M, male; n/a, not available.

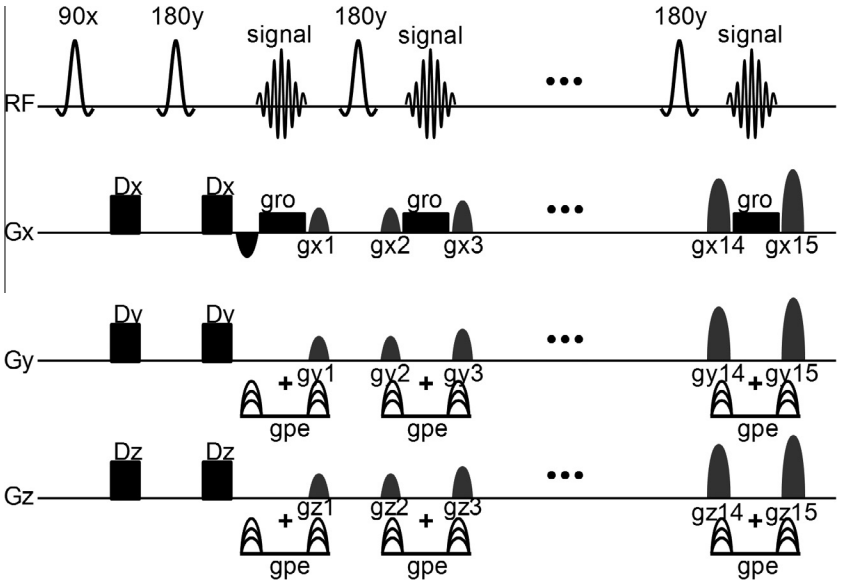

Fig. 2. Three-dimensional multiple spin echo DTI sequence were used for data acquisition of postmortem prenatal fetal brains. RF stood for radial frequency. Dx, Dy and Dz were gradients for diffusion weighting, gx1–gx15, gy1–gy15 and gz1–gz15 were crusher gradients. gro was the readout gradient and gpe was for phase encoding.

from 37 pcw and 3 year-old-subject was acquired at CMC. The data of all other postnatal subjects was acquired at AIRC. All subjects gave informed written consent approved by Institutional Review Board (IRB). No sedation was used for all data acquisition. DTI data were acquired using identical sequence as follows: single-shot echo planar imaging (EPI) with SENSE parallel imaging scheme (SENSitivity Encoding, reduction factor = 2.5); resolution of $2 \times 2 \times 2$ mm^3, 30 independent diffusion-weighted directions uniformly distributed in space, *b*-value of 1000 s/mm^2 and 2 repetitions. For DTI, the total acquisition time was 11 min. T1-weighted magnetization-prepared rapid gradient-echo (MPRAGE) image was also acquired. The MPRAGE images provided superior gray and white matter contrast for human brains during postnatal development except for the 37 pcw brain and were used for segmentation and parcellation of the cerebral cortex. T1-weighted and DTI images were acquired in the same session. The imaging parameters for MPRAGE were: TR = 8.3 ms, TE = 3.8 ms, flip angle = 12 , voxel size = $1 \times 1 \times 1$ mm^3, FOV = $256 \times 256 \times 160$ mm^3, scan time = 4 min.

2.5. DTI tractography to trace white matter tracts

For each subject, DTI datasets were first corrected for eddy current distortion using DTIStudio [43]. Specifically, DWIs from both repetitions were registered to a single b0 (non-diffusion sensitized) image using a 12-parameter (affine) linear image registration with automated image registration (AIR) algorithm [44]. FACT [34] tractography was conducted to trace the WM tracts of brains at all ages. The DTI tractography protocol in terms of placement and edition of ROIs for prenatal and postnatal brains followed Huang et al. [12,18] and Wakana et al. [45,46], respectively. For fiber tracing, a FA threshold of 0.15 for prenatal brains and the neonatal brain or 0.2 for children and adult brains and an inner product threshold of 0.75 were used. Diagrams of ROI operations for tractography and detailed procedures of using these ROI operations to trace a specific WM tract are demonstrated in Fig. 4. An ROI placement with "OR" operation extracts all fibers penetrating this ROI (Fig. 4a). With another ROI placement with "AND" operation, only kept fibers are those penetrating both green and orange ROIs (Fig. 4b). A third ROI placement with "NOT" operation removes fibers penetrating the red ROI (Fig. 4c). Left cingulum bundle in cingulate cortex of a 37 pcw brain was traced with these ROI operations, demonstrated in Fig. 4d–g. The 1st green ROI was placed with "OR" operation in the coronal slice crossed at splenium of corpus callosum (Fig. 4d) and traced yellow fibers were shown in Fig. 4e. 2nd ROI was placed with "AND" operation in the coronal slice crossed at genu of corpus callosum (Fig. 4f) and the left cingulum bundle in cingulate cortex was traced (Fig. 4g). The 3D reconstruction of this tract is shown in Fig. 4h. The above-mentioned fiber tracking procedures were also conducted by using DTIStudio [43].

The categorization of the traced tracts can be found in Table 2. The full tract names of the abbreviated ones described below can be also found in the legend of Table 2. The traced major tracts were categorized into 5 functionally distinctive tract groups, namely, limbic, brain stem, projection, commissural and association tract group. The categorization of the tracts into tract groups was introduced in the tract-based DTI atlas of adult human WM anatomy [45]. Such categorization was primarily based on the function of the tracts. Specifically, limbic tracts including cg and fx are those in the limbic system. Brain stem tracts are those connecting neural structures in the brain stem and cerebellum. Project tracts are those connecting cerebral cortex and brain stem or connecting cerebral cortex and thalamus. Commissural tracts with cc as the dominant one connect two cerebral hemispheres. Association tracts are those connecting two different cortical regions in the same cerebral hemisphere. Heterogeneous WM maturation processes were suggested based on findings from DTI tractography [e.g. 12,20]. DTI tractography provides a useful tool to visualize these heterogeneous morphological changes of the major WM fiber bundles during development.

2.6. Manual delineation of cortical regions of interests used for gene profiling

The cortical surfaces of prenatal brain specimens from 14 pcw to 19 pcw and *in vivo* brain around birth at 37 pcw were reconstructed with software (Amira, Mercury, San Diego, CA), based on the contrast of aDWI images. The cortical surface of *in vivo* brains from 3 years to 32 years was reconstructed with freesurfer [47], based on the contrast of T1 weighted images. Cortical ROIs were drawn by the operators who conducted micro-dissection for transcriptome analysis. Surface editing functions in Amira software were used to directly delineate these ROIs from the 3D

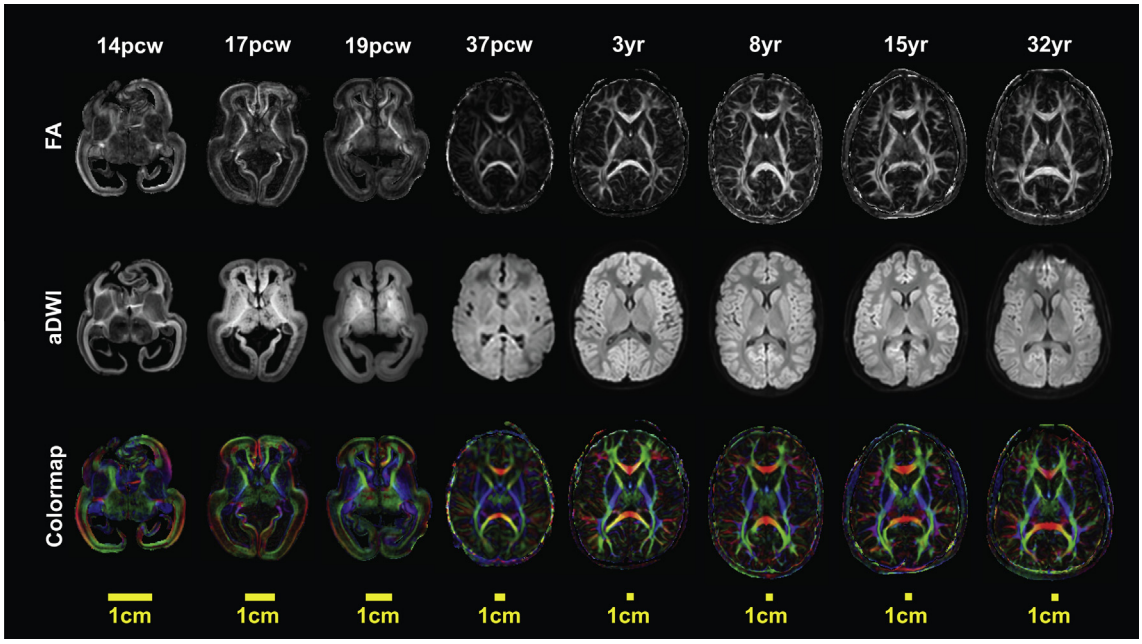

Fig. 3. Axial slices of the FA maps are shown in the top row, averaged DWIs (aDWI) are shown in the middle row, and color-encoded diffusion orientation maps are shown in the bottom row.

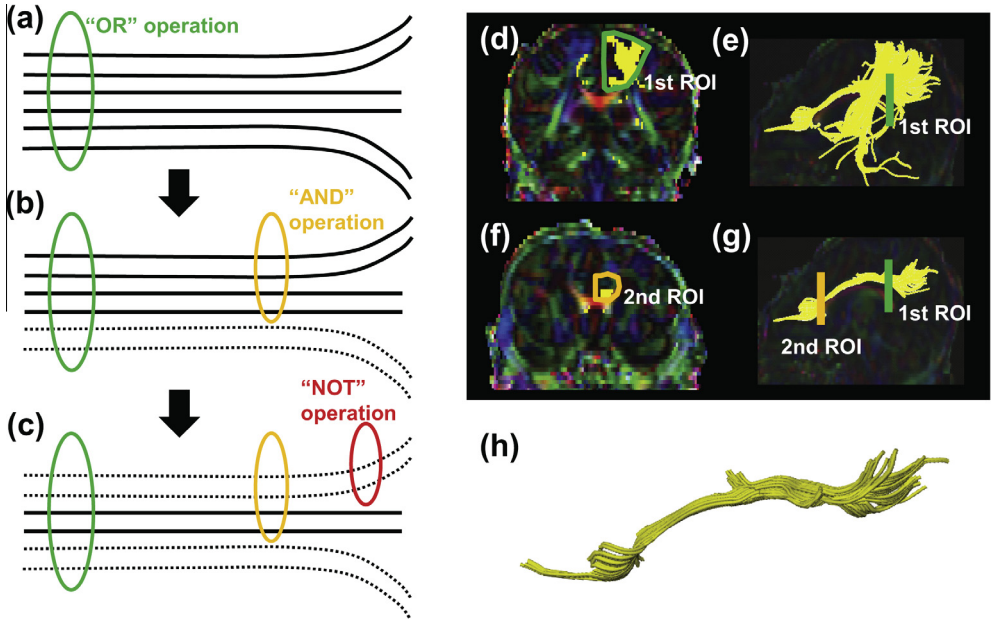

Fig. 4. Diagrams of "OR", "AND" and "NOT" operations with ROI placement for DTI tractography are shown in panel (a), (b) and (c), respectively. An example of tracing the left cingulum bundle in the cingulate cortex (cg-cx) of a 37 pcw brain with these ROI placement operations is demonstrated in panels (d)–(g). The 3D reconstructed cg-cx is illustrated in panel (h).

reconstructed cortical surface. The details of the ROI delineation protocol can be found in the literature [48]. Neocortical ROIs were manually placed on the neocortical surface of all prenatal brains examined and their anatomical positions were described in detail in the literature [2]. These ROIs represented the differential functional cortical areas including orbital prefrontal cortex (OFC), dorsolateral prefrontal cortex (DFC), medial prefrontal cortex (MFC), ventrolateral prefrontal cortex (VFC), primary motor cortex (M1C), primary somatosensory cortex (S1C), posteroinferior parietal cortex (IPC), primary auditory cortex (A1C), posterior superior temporal cortex (STC), inferior temporal cortex (ITC) and primary visual (occipital) cortex (V1C). Labeling of subcortical structures including striatum (STR), amygdaloid complex (AMY), hippocampus (HIP), mediodorsal nucleus of thalamus (MD), and cerebellar cortex (CBC) were also conducted with the DTI/MRI volume dataset, with the image segmentation function of Amira software.

2.7. Visualization of fiber tracts and cortical structures

The fiber tracts and cortical structures were converted into the simple legacy VTK file format (.vtk). The specification for this format can be found at http://www.vtk.org/VTK/img/file-formats.pdf. This format is supported directly by the Visualization Toolkit (VTK), which is a powerful and flexible C++ library for graphically

Table 2
Categorization of the major white matter tracts into 5 functionally distinctive tract groups.

Limbic tract group	cg-cx, cg-tx, fx
Brain stem tract group	icp, mcp, scp
Projection tract group	csp, ic, athr, pthr, sthr
Commissural tract group	ac, cc
Association tract group	ec, gef, ilf, offi, slf, unf

Abbreviation of the tract names: ac: anterior commissure; athr/sthr/pthr: anterior, superior and posterior thalamic radiation; cc: corpus callosum; cg-cx: cingulum bundle in cingulate cortex; cg-tx: cingulum bundle in temporal cortex; csp: corticospinal tract; ec: external capsule; fx: fornix; gef: ganglionic eminence fibers; ic: internal capsule; icp/mcp/scp: inferior/middle/superior cerebellar peduncle; ilf/slf: inferior and superior longitudinal fasciculus; offi: inferior occipitofrontal fasciculus; saf: short association fibers, uncinate fasciculus (unf).

displaying data. While it is possible to write custom VTK code to import and display the annotated fiber tract files, we used an easier alternative with Paraview (http://www.paraview.org/paraview/resources/software.php), a free desktop data visualization application that supports the VTK file format, and demonstrated all the 3D fibers (Figs. 5–10 below) with Paraview. "Tube" option in Paraview was used to display all the WM fibers.

3. Results

All data presented below (except Fig. 10) is downloadable from the website http://www.brainspan.org/static/download.html.

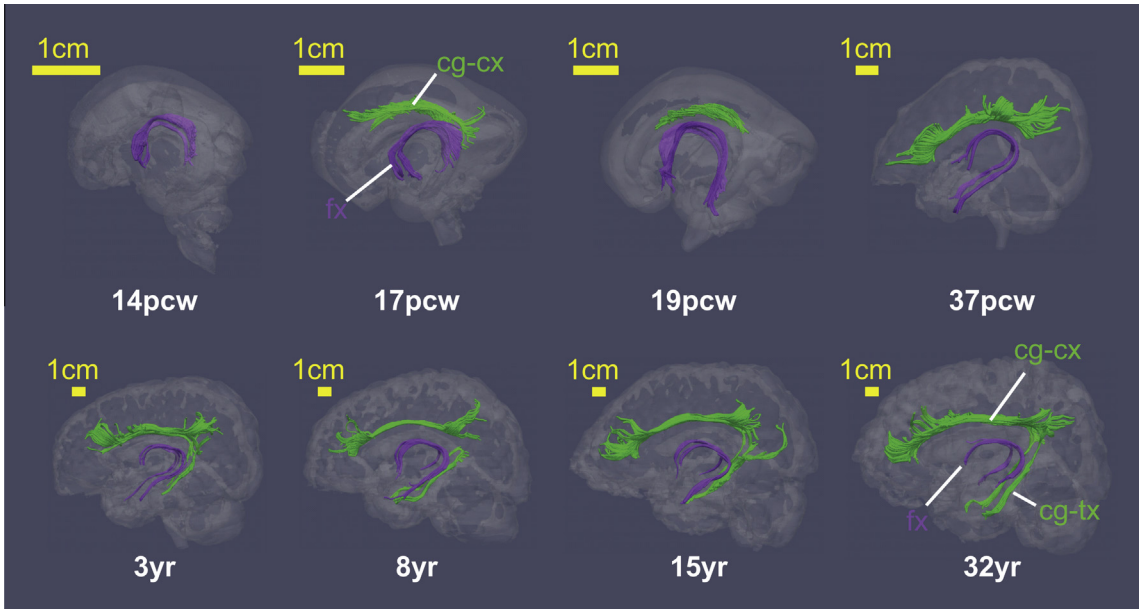

Fig. 5. Limbic fibers including cingulum bundle in the cingulate cortex (cg-cx), cingulum bundle in the temporal cortex (cg-tx) and fornix (fx) for brains from 14 pcw to 32 years.

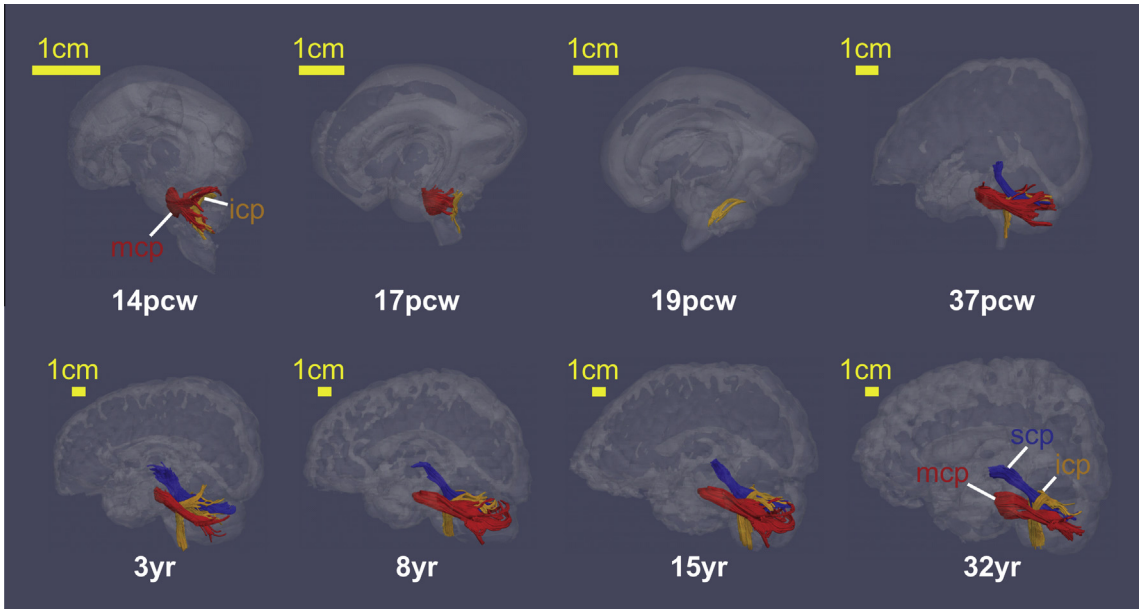

Fig. 6. Brainstem fibers including inferior, middle and superior cerebellar peduncle (icp, mcp and scp) for brains from 14 pcw to 32 years.

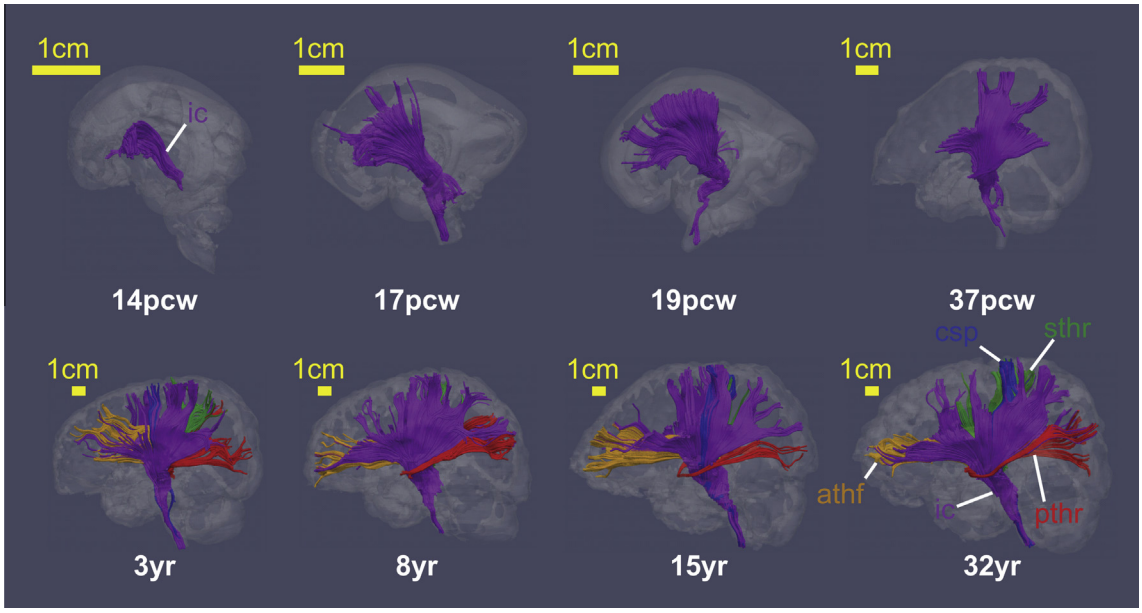

Fig. 7. Projection fibers including interior capsule (ic), corticospinal tract (csp), anterior, superior and posterior thalamic radiation (atr, str and ptr) for brains from 14 pcw to 32 years.

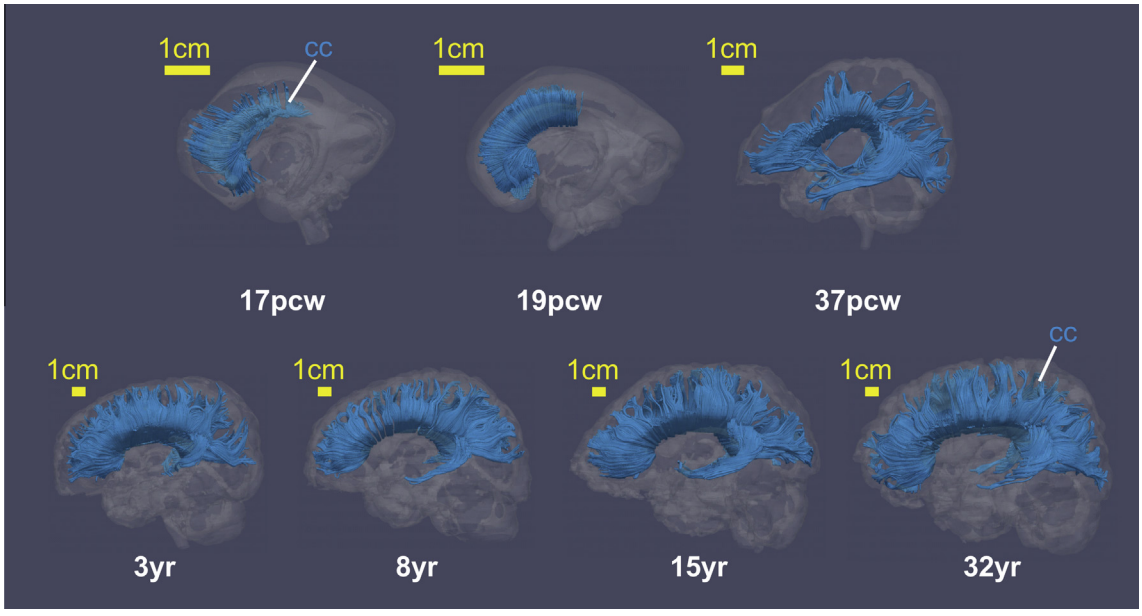

Fig. 8. Corpus callosum (cc) for brains from 17 pcw to 32 years.

3.1. Developmental changes of DTI-derived maps

Various DTI-derived maps of developing brains from early fetal stage at 14 pcw to adulthood at 32 years, including FA, averaged DWIs (aDWIs), and color-encoded maps, are shown in Fig. 3. Axial slices were selected based on anatomical similarities at each developmental stage. DTI-derived maps directly demonstrate overall macrostructural and microstructural changes of developing human brain. The aDWIs of brain specimens from 14 pcw to 19 pcw show clearly the smooth cortical surfaces and lack of gyrification. It can be appreciated with these axial images that the ventricular size relative to the brain size of developing brains from 14 pcw to 19 pcw is significantly larger than that of brains from 37 pcw to 32 years, and the relative size of the ventricle appears to be decreasing during prenatal development. Clear differentiation of the three layers in the cerebral wall of the fetal brains from 14 pcw to 19 pcw can be seen in the FA maps with the bright–dark–bright contrast from outmost to innermost of the cerebral wall. The most superficial layer, the cortical plate, has a relatively high FA at 14 pcw, but decreases from 14 pcw to 37 pcw. The subplate FA just below the cortical plate remains low throughout development into 37 pcw. Cortical FA is consistently low from 37 pcw to 32 years. WM FA becomes brighter from 14 pcw to 32 years. Similarity of the color-encoded map across 37 pcw–32 years suggests that most of major WM tracts exist around birth (37 pcw). This developmental character of the major WM tracts can be clearly appreciated with the 3D reconstructed fibers in Figs. 5–9 below.

Please cite this article in press as: A. Ouyang et al., Methods (2014), http://dx.doi.org/10.1016/j.ymeth.2014.10.025

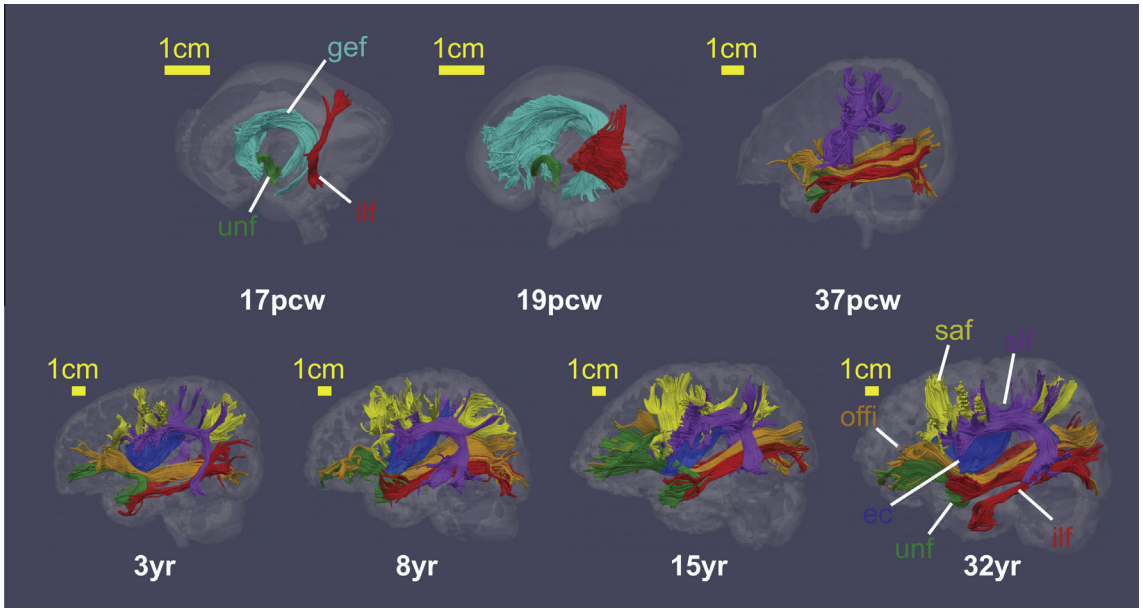

Fig. 9. Association fibers including fibers in external capsule (ec), ganglionic eminence (gef), inferior longitudinal fasciculus (ilf), inferior occipitofrontal fasciculus (offi), short association fibers (saf), superior longitudinal fasciculus (slf) and uncinated fasciculus (unf) for brains from 17 pcw to 32 years.

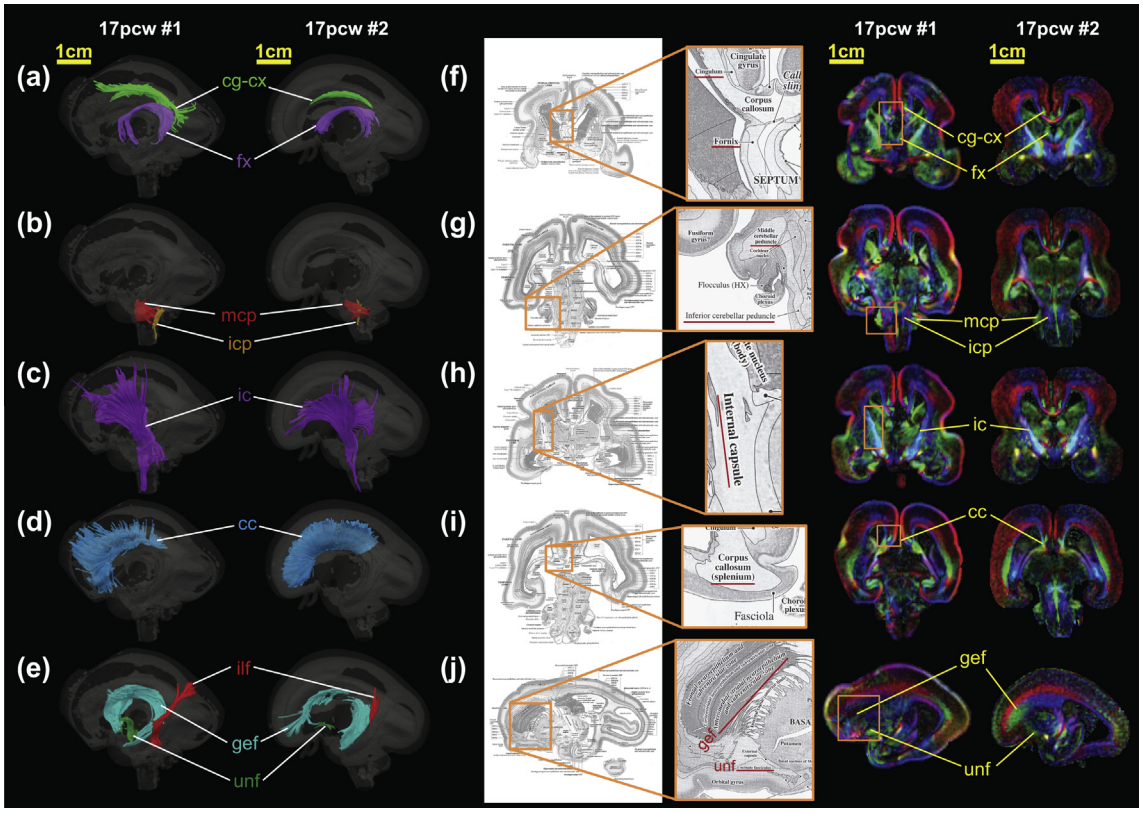

Fig. 10. 3D reconstructed limbic (a), brain stem (b), projection (c), callosal (d) and association (e) WM tracts of two 17 pcw fetal brain specimens demonstrate reproducibility of these traced tracts at a specific gestational age. Panels (f)–(j) show the histological findings of these same tracts in a 17 pcw fetal brain and their anatomical locations in the 2D (f–g: coronal; j: sagittal) color-encoded diffusion orientation maps of the same two 17 pcw fetal brain specimens. The histological images were adapted from the published atlas [15].

3.2. DTI tractography results for different tract groups

3.2.1. Limbic system tracts

Limbic system tracts include primarily fx, cg-cx and cg-tx. As shown in Fig. 5, limbic system fibers appear early during development. As early as 14 pcw, the entire fx could be traced with DTI tractography. Also shown in Fig. 5, for the brain specimen at 17 pcw, both fx and cg-cx could be delineated with DTI tractography. cg-cx is not apparent in 14 pcw and could not be traced. All limbic fibers could be reproducibly traced from postnatal 3 years to 32 years. cg-tx could not be traced for the 37 pcw brain probably due to the partial volume effects. During this long developmental

period from early 14 pcw to adulthood, the overall shape of the limbic system fibers appears relatively stable without any major changes in morphology.

3.2.2. Brainstem tracts

Major brainstem tracts include mcp, icp, and scp and are also among those WM fibers appearing early during brain development. As can be observed in Fig. 6, mcp and icp could be traced for the fetal brain as early as 14 pcw. They were also successfully traced in the fetal brain at 17 pcw. The mcp could not be traced for the 19 pcw brain due to damage of the cerebellar tissue in this sample. All major brainstem fibers could be reproducibly traced and retained similar morphology for brains from 37 pcw to 32 years.

3.2.3. Projection tracts

Projection tracts include those connecting between brain stem or thalamus to cerebral cortex. WM tracts connecting brain stem mainly consist of ic, which include csp as the fibers projecting to the motor cortex. WM tracts connecting the thalamus include athr, sthr and pthr, which are anterior, superior and posterior part of thalamic fibers connecting to cerebral cortex. As shown in Fig. 7, ic is among the fibers that appear early and can be traced for fetal brain as early as 14 pcw. The general maturation pattern for ic is from anterior to posterior of the brain during prenatal brain development from 14 pcw to 37 pcw. All above-mentioned projection fibers could be reproducibly traced from postnatal 3 years to 32 years.

3.2.4. Commissural tracts

Major commissural tracts include cc and ac. As shown in Fig. 3, cc and ac can be observed with a color-encoded diffusion orientation map of the 14 pcw brain, but they could not be traced with DTI tractography. Only traced cc of developing brains is shown in Fig. 8, as ac contains branching fibers which cannot be reproducibly traced with FACT [34] algorithm. Anterior part of cc has been well delineated for brain at 17 pcw with DTI tractography (Fig. 8). There is a general anterior to posterior maturation pattern for cc of prenatal brains from 17 pcw to 37 pcw. Tapetum of cc projecting to the temporal lobe could not be traced for brains at 17 pcw and 19 pcw. The entire cc including tapetum could be well delineated for brains from 37 pcw to 32 years.

3.2.5. Association tracts

Association tracts include ec, ilf, offi, saf, slf, unf and gef, representing the fibers connecting between two different cortical regions. gef is a transient fetal brain structure with coherent fiber bundles running inside it. As shown in Fig. 9, the fibers of ge can be only traced in the brain at 17 pcw and 19 pcw. unf and ilf appear earliest among all association tracts and both can be traced in the brain at 17 pcw; however, ilf and offi could not be separately traced in the brain at 19 pcw. Significant association fiber maturation can be observed in brains during prenatal development. The most dramatic morphological change of postnatal development of association tracts is the maturation of the arcuate fasciculus, part of slf connecting temporal lobe to other cortical regions. Except arcuate fasciculus, other major components of slf could be well traced for brain at 37 pcw. saf could not be traced for 37 pcw brain possibly due to partial volume effects. After 3 years, the association fibers become relatively stable and all above-mentioned association tracts (except gef) can be reproducibly traced from 3 years to 32 years.

Reproducibility of the traced tracts and consistency of DTI tractography to histology reproducibility of the DTI tractography for tracing major tracts can be demonstrated in Fig. 10a to Fig. 10e, showing traced limbic (Fig. 10a), brain stem (Fig. 10b), projection (Fig. 10c), callosal (Fig. 10d) and association tracts (Fig. 10e) of two 17 pcw fetal brain specimens with similar 3D morphology. Furthermore, these tracts can also be identified with histological images [15] and corresponding DTI color-encoded diffusion orientation maps of both 17 pcw fetal brain specimens (Fig. 10f–j), indicating consistency of the WM neuroanatomy revealed from DTI to that revealed from histology

4. Discussion

In this study, the macrostructural morphological changes of major WM tracts have been revealed for developmental brains from early fetal stage at 14 pcw to adulthood at 32 years with DTI. Previous research has explored the developmental changes of WM fibers during either prenatal ([e.g. 12,20]) or postnatal period ([e.g. 49–52]) separately, but not across both periods. Despite limited sample number and qualitative characterization, this study may have presented the first structural and connectional mapping of the human brain with such a comprehensive age range covering prenatal and postnatal development. DTI was acquired from prenatal *ex vivo* specimens and postnatal *in vivo* subjects. The WM tracts were categorized into five functional tract groups. DTI tractography has been used to effectively reveal the heterogeneous maturation patterns of different tract groups. ROIs drawn on the cortical surface delineated regions where tissues were dissected for gene profiling and establishing a developing transcriptome atlas. The paper described the methods of DTI data acquisition, DTI tractography and cortical surface mapping for developing brains. The outcome of these methods is the spatial mapping of the structural and connectional imaging data that serves as anatomical backbone for the transcriptional atlas of developing human brain.

Two most prominent features can be directly observed from the two-dimensional axial FA, aDWI and color-coded diffusion orientation maps of developing brains from 14 pcw to 32 years in Fig. 3. One is relatively high FA in the cortical plate from 14 pcw to 19 pcw. The cortical FA is low around birth at 37 pcw and remains low from 37 pcw to 32 years. In the fetal stage, FA values of the cortical plate are high [e.g. 13,48,53–63] due to the dominant organized radial glial scaffold in the cortex. The disruption of the columnar structures caused by loss of radial glia, synapse formation and increased dendritic density [e.g. 48,56,62] leads to a decrease in FA values. The second prominent feature is that relatively smooth cortical surfaces can be appreciated for fetal brains from 14 pcw to 19 pcw with only the Sylvian fissure clearly identifiable from axial maps of these brains.

Noninvasive DTI tractography has a great advantage for delineating qualitative morphological changes of major fiber bundles during brain development. With the brain WM tracts categorized into different functional tract groups, the dynamics of morphological changes of these distinctive tract groups can be appreciated from Figs. 5–9. In general, limbic and brain stem tracts appear early and association tracts appear latest among all tract groups. The morphology of limbic tracts is also relatively more stable compared to other tracts. For example, the "C"-shaped fornix could be traced for the brain as early as 14 pcw. This "C"-shape remains relatively consistent throughout the middle-late fetal and postnatal development. On the contrary, ic and cc in projection and commissural tract group, respectively, undergoes an anterior-to-posterior extension pattern. Association tracts such as slf have the most dynamic morphological changes among all tract groups. ge is a temporary neural structure only existing in the prenatal human brain. The presence of the coherent fibers inside ge before term shown in Fig. 9 and our previous publication [18] is consistent to the description that the medial ge transports interneurons perpendicular to the radial glia in the literature [64,65]. Coherent fibers in ge could not be traced for the brain at 37 pcw, around normal birth time. The adopted DTI-based tractography method, FACT, is a widely used deterministic line propagation method. Although it is known that FACT cannot resolve

Please cite this article in press as: A. Ouyang et al., Methods (2014), http://dx.doi.org/10.1016/j.ymeth.2014.10.025

crossing or branching fibers, it is effective in characterizing major WM fiber bundles after it is combined with brute force and multi-ROI approach [66].

The anatomical information from advanced neural imaging techniques such as high resolution DTI serves as the anatomical backbone for the transcriptional atlas. In the future, it is possible to set up a one-to-one correspondence between structural measurement and gene expression at specific cortical locations. Integrating the information from DTI/MRI and gene profiling will have multiple advantages of accessing complicated brain developmental processes. First, associating the cortical map of gene expression profiling to the cortical map of structural measurements helps explain why orderly structural changes occur. Second, DTI/MRI is a noninvasive approach. With the advent of ever more sophisticated MRI technology, high-quality DTI/MRI data will become readily available. These advances of DTI/MRI technologies provide the possibility of obtaining the sophisticated structural information from not only the *in vivo* postnatal developing brains but also *in vivo* prenatal fetal brains (with *in utero* DTI/MRI) noninvasively. Establishing the correlation between DTI and gene profiling could potentially help interpret structural measurements from DTI/MRI with gene expression, and vice versa.

There are several limitations of this study. DTI tractography cannot differentiate anterograde and retrograde directions, so projection tract group includes fibers in both directions, i.e. those projecting from brain stem and thalamus to the cerebral cortex and those from cerebral cortex to subcortical structures. The demonstrated results are mixed ones from both *ex vivo* and *in vivo* DTI data which were acquired with the MR scanners of different magnetic strengths. With current MR technology limitations, it is still not practical to acquire *in vivo* fetal brain DTI with the high resolution presented in this study from a clinical MR system. Due to these limitations, only qualitative description of the macrostructural anatomy of the developing brain from the perspective of DTI tractography was presented, as the tractography of WM fibers from a deterministic tracing method is not sensitive to differences of magnetic strengths or acquisition protocols given sufficient signal-to-noise ratio and resolution of the data. Deterministic tractography is controlled by two parameters, FA and primary eigenvector of diffusion tensor. It has been proved that FA, as a relative index, is not sensitive to fixation [i.e. [67,68]]. In addition, the primary eigenvector is not sensitive to differences of magnetic strength and imaging protocol. For example, the color-encoded diffusion orientation maps of the brain stem from *in vivo* DTI acquired with a 1.5 T scanner and from *ex vivo* DTI acquired with an 11.7 T scanner demonstrate similar contrast in a recent study [69]. Besides our tractography study with postmortem fetal brain samples, similar studies of postmortem fetal brain samples [20,63] also demonstrated that the tractography could reflect the underlying WM fiber pathways. DTI tractography, however, is sensitive to the factors such as image resolution, myelination and coherence of the WM fibers. Some fibers, such as cc of 14 pcw brain, can be well appreciated in the DTI color-encoded map (Fig. 3), but cannot be traced with DTI tractography (Fig. 8) possibly due to these factors. The sources of variability of DTI tractography of postmortem fetal brain specimens could also be related to fixation and tissue damage. For example, mcp was identified in the histological atlas of the 19 pcw brain [15], but we were not able to successfully trace mcp of the postmortem 19 pcw brain in the Fig. 6 as the cerebellum and brain stem were among the neural structures most easily damaged during the processes of specimen preparation or transportation. Despite the limitations especially related to *ex vivo* DTI of postmortem fetal brain specimens, Fig. 10 demonstrates that the overall morphology of major WM tracts revealed from DTI tractography is reproducible in different brain specimens and consistent to the histological findings. Small fibers, such as "U"-shaped fibers in peripheral WM, are difficult to trace with the current image resolution and limitations of DTI tractography algorithms including FACT. Therefore, we did not include tractography of any such fiber in this paper. There is no quantitative DTI methods described in this paper. Although several DTI derived metrics, such as axial or radial diffusivity, offer unique quantitative and microstructural insight into both cortical and WM development, the differences of *ex vivo* and *in vivo* DTI and MR scanners can result in significant biases on these microstructural measurements. The number of samples is limited and it makes quantitative and statistical analysis of structural development with DTI/MRI not possible.

5. Conclusion

DTI imaging and tractography have provided an effective means for noninvasively characterizing the anatomical and connectional changes of developing brains from early fetal stage to adulthood. The heterogeneous formation and maturation processes of WM tracts categorized into five functional tract groups have been revealed. Reproducibility of the major tracts traced with DTI tractography and consistency of these traced tracts to the histological findings were also illustrated. The structural and connectional imaging data offered by DTI provides an anatomical backbone of transcriptional atlas of the developing human brain (www.brainspan.org).

Acknowledgments

This study is sponsored by NIH grants MH092535, MH092535S1, MH089921, MH081896, MH089929 and NS051869.

References

[1] M.B. Johnson, Y.I. Kawasaw, C.E. Mason, Z. Krsnik, G. Coppola, D. Bogdanovic, D.H. Geschwind, S.M. Mane, M.W. State, N. Sestan, Neuron 62 (2009) 494–509.
[2] H.J. Kang, Y.I. Kawasawa, F. Cheng, Y. Zhu, X. Xu, M. Li, A.M.M. Sousa, M. Pletikos, K.A. Meyer, G. Sedmak, T. Guennel, Y. Shin, M.B. Johnson, Z. Krsnik, S. Mayer, S. Fertuzinhos, S. Umlauf, S.N. Lisgo, A. Vortmeyer, D.R. Weinberger, S. Mane, T.M. Hyde, A. Huttner, M. Reimers, J.E. Kleinman, N. Sestan, Nature 478 (2011) 483–489.
[3] M. Pletikos, A.M.M. Sousa, G. Sedmak, K.A. Meyer, Y. Zhu, F. Cheng, M. Li, Y. Kawasawa, N. Sestan, Neuron 81 (2014) 321–332.
[4] E.S. Lein, M.J. Hawrylycz, N. Ao, M. Ayres, A. Bensinger, A. Bernard, A.F. Boe, M.S. Boguski, K.S. Brockway, E.J. Byrnes, L. Chen, L. Chen, T.M. Chen, M.C. Chin, J. Chong, B.E. Crook, A. Czaplinska, C.N. Dang, S. Datta, N.R. Dee, A.L. Desaki, T. Desta, E. Diep, T.A. Dolbeare, M.J. Donelan, H.W. Dong, J.G. Dougherty, B.J. Duncan, A.J. Ebbert, G. Eichele, L.K. Estin, C. Faber, B.A. Facer, R. Fields, S.R. Fischer, T.P. Fliss, C. Frensley, S.N. Gates, K.J. Glattfelder, K.R. Halverson, M.R. Hart, J.G. Hohmann, M.P. Howell, D.P. Jeung, R.A. Johnson, P.T. Karr, R. Kawal, J.M. Kidney, R.H. Knapik, C.L. Kuan, J.H. Lake, A.R. Laramee, K.D. Larsen, C. Lau, T.A. Lemon, A.J. Liang, Y. Liu, L.T. Luong, J. Michaels, J.J. Morgan, R.J. Morgan, M.T. Mortrud, N.F. Mosqueda, L.L. Ng, R. Ng, G.J. Orta, C.C. Overly, T.H. Pak, S.E. Parry, S.D. Pathak, O.C. Pearson, R.B. Puchalski, Z.L. Riley, H.R. Rockett, S.A. Rowland, J.J. Royall, M.J. Ruiz, N.R. Sarno, K. Schaffnit, N.V. Shapovalova, T. Sivisay, C.R. Slaughterbeck, S.C. Smith, K.A. Smith, B.I. Smith, A.J. Sodt, N.N. Stewart, K.R. Stumpf, S.M. Sunkin, M. Sutram, A. Tam, C.D. Teemer, C. Thaller, C.L. Thompson, L.R. Varnam, A. Visel, R.M. Whitlock, P.E. Wohnoutka, C.K. Wolkey, V.Y. Wong, M. Wood, M.B. Yaylaoglu, R.C. Young, B.L. Youngstrom, X.F. Yuan, B. Zhang, T.A. Zwingman, A.R. Jones, Nature 445 (2007) 168–176.
[5] P. Rakic, J. Comp. Neurol. 145 (1972) 61–83.
[6] P. Rakic, Science 241 (1988) 170–176.
[7] R.L. Sidman, P. Rakic, Brain Res. 62 (1973) 1–35.
[8] R.L. Sidman, P. Rakic, in: W. Haymaker, R.D. Adams (Eds.), Histology and Histopathology of the Nervous System, Springfield, Illinois, 1982, pp. 3–145.
[9] L.S. Honig, K. Herrmann, C.J. Shatz, Cereb. Cortex 6 (1996) 794–806.
[10] J.J. Volpe, Pediatr. Res. 50 (2001) 553–562.
[11] P.J. Basser, J. Mattiello, D.L. Bihan, Biophys. J. 66 (1994) 259–267.
[12] H. Huang, R. Xue, J. Zhang, T. Ren, L.J. Richards, P. Yarowsky, M.I. Miller, S. Mori, J. Neurosci. 29 (2009) 4263–4273.
[13] H. Huang, L. Vasung, Int. J. Dev. Neurosci. 32 (2014) 11–22.
[14] S.A. Bayer, J. Altman, The Human Brain During the Third Trimester, CRC, Boca Raton, FL, 2004.
[15] S.A. Bayer, J. Altman, The Human Brain During the Second Trimester, CRC, Boca Raton, FL, 2005.
[16] I. Kostovic, P.S. Goldman-Rakic, J. Comp. Neurol. 219 (1983) 431–447.
[17] I. Kostovic, Neuroscience 17 (1986) 1047–1077.

[18] H. Huang, J. Zhang, S. Wakana, W. Zhang, T. Ren, L.J. Richards, P. Yarowsky, P. Donohue, E. Graham, P.C.M. van Zijl, S. Mori, Neuroimage 33 (2006) 27–38.
[19] H. Huang, Neuroscientist 16 (2010) 634–649.
[20] E. Takahashi, R.D. Folkerth, A.M. Galaburda, P.E. Grant, Cereb. Cortex 22 (2012) 455–464.
[21] J. Zhang, A. Evans, L. Hermove, S.K. Lee, S. Wakana, W. Zhang, P. Donohue, M.I. Miller, H. Huang, X. Want, P.C. van Zijl, S. Mori, Neuroimage 38 (2007) 239–247.
[22] K. Oishi, S. Mori, P.K. Donohue, T. Ernst, L. Anderson, S. Buchthal, A. Faria, H. Jiang, X. Li, M.I. Miller, P.C. van Zijl, L. Chang, Neuroimage 56 (2011) 8–20.
[23] G.M. Innocenti, Science 212 (1981) 824–826.
[24] W.M. Cowan, J.W. Fawcett, D.D.M. O'Leary, B.B. Stanfield, Science 225 (1984) 1258–1265.
[25] G.M. Innocenti, D.J. Price, Nat. Rev. Neurosci. 6 (2005) 955–965.
[26] A.S. LaMantia, P. Rakic, J. Neurosci. 10 (1990) 2156–2175.
[27] A.S. LaMantia, P. Rakic, J. Comp. Neurol. 340 (1994) 328–336.
[28] T.U. Woo, M.L. Pucak, C.H. Kye, C.V. Matus, D.A. Lewis, Neuroscience 80 (1997) 1149–1158.
[29] E.O. Stejskal, J.E. Tanner, J. Chem. Phys. 42 (1965) 288.
[30] P.J. Basser, C. Pierpaoli, J. Magn. Res. 111 (1996) 209–219.
[31] P.J. Basser, D.K. Jones, NMR Biomed. 15 (2002) 456–467.
[32] C. Beaulieu, NMR Biomed. 15 (2002) 435–455.
[33] S. Mori, J. Zhang, Neuron 51 (2006) 527–539.
[34] S. Mori, B.J. Crain, V.P. Chacko, P. van Zijl, Ann. Neurol. 45 (1999) 265–269.
[35] T.E. Conturo, N.F. Lori, T.S. Cull, E. Akbudak, A.Z. Snyder, J.S. Shimony, R.C. McKinstry, H. Burton, M.E. Raichle, Proc. Natl. Acad. Sci. U.S.A. 96 (1999) 10422–10427.
[36] D.K. Jones, A. Simmons, S.C. Williams, M.A. Horsfield, Magn. Reson. Med. 42 (1999) 37–41.
[37] P.J. Basser, S. Pajevic, C. Pierpaoli, J. Duda, A. Aldroubi, Magn. Reson. Med. 44 (2000) 625–632.
[38] C. Poupon, C.A. Clark, V. Frouin, J. Regis, L. Bloch, D. Le Bihan, J.F. Mangin, Neuroimage 12 (2000) 184–195.
[39] G.J.M. Parker, C.A.M. Wheeler-Kingshott, G.J. Barker, IEEE Trans. Med. Imaging 21 (2002) 505–512.
[40] M. Lazar, D.M. Weinstein, J.S. Tsuruda, K.M. Hasan, K. Arfanakis, M.E. Meyerand, B. Badie, H.A. Rowley, V. Haughton, A. Field, A.L. Alexander, Hum. Brain Mapp. 18 (2003) 306–321.
[41] B. Stieltjes, W.E. Kaufmann, P.C.M. van Zijl, K. Fredericksen, G.G. Pearlson, S. Mori, Neuroimage 14 (2001) 723–735.
[42] M. Catani, R.J. Howard, S. Pajevic, D.K. Jones, Neuroimage 17 (2002) 77–94.
[43] H. Jiang, P.C.J.K. van Zijl, G.D. Pearlson, S. Mori, Comput. Methods Programs Biomed. 81 (2006) 106–116.
[44] R.P. Woods, S.T. Grafton, C.J. Holmes, S.R. Cherry, J.C. Mazziotta, J. Comput. Assist. Tomogr. 22 (1998) 139–152.
[45] S. Wakana, H. Jiang, L.M. Nagae-Poetscher, P.C. van Zijl, S. Mori, Radiology 230 (2004) 77–87.
[46] S. Wakana, A. Caprihan, M.M. Panzenboeck, J.H. Fallon, M. Perry, R.L. Gollub, K. Hua, J. Zhang, H. Jiang, P. Dubey, A. Blitz, P. van Zijl, S. Mori, Neuroimage 36 (2007) 630–644.
[47] B. Fischl, A.M. Dale, Proc. Natl. Acad. Sci. U.S.A. 97 (2000) 11044–11049.
[48] H. Huang, T. Jeon, G. Sedmak, M. Pletikos, L. Vasung, X. Xu, P. Yarowsky, L. Richards, I. Kostovic, N. Sestan, S. Mori, Cereb. Cortex 23 (2013) 2620–2631.
[49] N. Barnea-Goraly, V. Menon, M. Eckert, L. Tamm, R. Bammer, A. Karchemskiy, C.C. Dant, A.L. Reiss, Cereb. Cortex 15 (2005) 1848–1854.
[50] J. Dubois, G. Dehaene-Lambertz, M. Perrin, J.F. Mangin, Y. Cointepas, E. Duchesnay, D. LeBihan, L. Hertz-Pannier, Hum. Brain Mapp. 29 (2008) 14–27.
[51] T.J. Eluvathingal, K.M. Hasan, L. Kramer, J.M. Fletcher, L. Ewing-Cobbs, Cereb. Cortex 17 (2007) 2760–2768.
[52] C. Level, L. Walker, A. Leemans, L. Phillips, C. Beaulieu, Neuroimage 40 (2008) 1044–1055.
[53] J.S. Thornton, R.J. Ordidge, J. Penrice, E.B. Cady, P.N. Amess, S. Punwani, M. Clemence, J.S. Wyatt, Magn. Res. Imaging 15 (1997) 433–440.
[54] J. Neil, S. Shiran, R. McKinstry, G. Schefft, A. Snyder, C. Almli, E. Akbudak, J. Arnovitz, J. Miller, B. Lee, T. Conturo, Radiology 209 (1998) 57–66.
[55] S. Mori, R. Itoh, J. Zhang, W.E. Kaufmann, P.C.M. van Zijl, M. Solaiyappan, P. Yarowsky, Magn. Reson. Med. 46 (2001) 18–23.
[56] R.C. McKinstry, A. Mathur, J.H. Miller, A. Ozcan, A.Z. Snyder, G.L. Schefft, C.R. Almli, S.I. Shiran, T.E. Conturo, J.J. Neil, Cereb. Cortex 12 (2002) 1237–1243.
[57] L.C. Maas, P. Mukherjee, J. Carballido-Gamio, S. Veeraraghavan, S.P. Miller, S.C. Partridge, R.G. Henry, A.J. Barkovich, D.B. Vigneron, Neuroimage 22 (2004) 1134–1140.
[58] A.R. Deipolyi, P. Mukherjee, K. Gill, R.G. Henry, S.C. Partridge, S. Veeraraghavan, H. Jin, Y. Lu, S.P. Miller, D.M. Ferriero, D.B. Vigneron, A.J. Barkovich, Neuroimage 27 (2005) 579–586.
[59] C.D. Kroenke, D.C. Van Essen, T.E. Inder, S. Rees, G.L. Bretthorst, J.J. Neil, J. Neurosci. 27 (2007) 12506–12515.
[60] S.V. Sizonenko, E.J. Camm, J.R. Garbow, S.E. Maier, T.E. Inder, C.E. Williams, J.J. Neil, P.S. Huppi, Cereb. Cortex 17 (2007) 2609–2617.
[61] C.D. Kroenke, E.N. Taber, L.A. Leigland, A.K. Knutsen, P.V. Bayly, Cereb. Cortex 19 (2009) 2916–2929.
[62] H. Huang, A. Yamamoto, M.A. Hossain, L. Younes, S. Mori, J. Neurosci. 28 (2008) 1427–1433.
[63] E. Takahashi, G. Dai, G.D. Rosen, R. Wang, K. Ohki, R.D. Folkerth, A.M. Galaburda, V.J. Wedeen, P. Ellen, Cereb. Cortex 21 (2011) 200–211.
[64] A.A. Lavdas, M. Grigoriou, V. Pachnis, J.G. Parnavelas, J. Neurosci. 19 (1999) 7881–7888.
[65] H. Wichterle, J.M. Garcia-Verdugo, D.G. Herrera, A. Alvarez-Buylla, Nat. Neurosci. 2 (1999) 461–466.
[66] H. Huang, J. Zhang, P.C. van Zijl, S. Mori, Magn. Reson. Med. 52 (2004) 559–565.
[67] S. Kim, J.J. Neil, S. Song, Magn. Reson. Med. 50 (2003) 743–748.
[68] J.H. Kim, K. Trinkaus, A. Ozcan, M.D. Budde, S. Song, NMR Biomed. 20 (2006) 352–359.
[69] M. Aggarwal, J. Zhang, O. Pletnikova, B. Crain, J. Trocoso, S. Mori, Neuroimage 74 (2013) 117–127.

Please cite this article in press as: A. Ouyang et al., Methods (2014), http://dx.doi.org/10.1016/j.ymeth.2014.10.025